

Methodology to assess phasor measurement unit in the estimation of dynamic line rating

ISSN 1751-8687

Received on 27th April 2017

Revised 15th March 2018

Accepted on 11th May 2018

E-First on 30th July 2018

doi: 10.1049/iet-gtd.2017.0661

www.ietdl.org

David L. Alvarez¹ ✉, F. Faria da Silva², Claus Leth Bak², Enrique E. Mombello³, Javier A. Rosero¹, Daniel Leó Ólason⁴

¹Electrical Machines & Drives Group, EM&D, Universidad Nacional de Colombia, Bogotá, Colombia

²Department of Energy Technology, Aalborg University, Aalborg, Denmark

³Instituto de Energía Eléctrica, CONICET, Universidad Nacional de San Juan, San Juan, Argentina

⁴LANDSNET, Iceland

✉ E-mail: dlalvarez@unal.edu.co

Abstract: This paper presents a methodology to analyse the influence of both atmospheric variations in time and space and the error in synchrophasor measurements to estimate conductor temperature along an overhead line. In this methodology, expressions to compute the error propagation in the computing of temperature because of measurement errors and load variations are proposed. The analysis begins by computing overhead line's thermal and mechanical parameters using simulations of load and atmospheric conditions. Having computed these parameters, values of resistance, inductance and capacitance of the overhead line modelled by means of a π equivalent circuit are estimated, with the purpose of quantifying the sensibility of electrical parameters to changes in conductor temperature. Additionally, this analysis allows the identification of the temperature in each span along OHLs. Subsequently, the average conductor temperature is estimated using simulations of synchrophasors through the relationship between resistivity and temperature. This estimated temperature is compared with the temperature computed using atmospheric conditions to obtain the maximum error. This error is contrasted with the acceptable error margins. Thus, during the planning stage, this methodology can be used to assess PMU as a method of computing conductor temperature.

1 Introduction

Power systems are facing new challenges in operation, control and planning. To better face these challenges, it is necessary to optimise assets capacity, because they have reached their limits as a consequence of new loads and sources [1]. These new loads and sources increase congestion and risk, especially in overhead lines (OHLs) [2]. Thus, to push limits in OHLs, new technologies and methods have been developed with the aim of improving their capacity, reliability, safety and economic operation [3]. Among these technologies is dynamic line rating (DLR) which has the ability to compute conductor's ampacity in real time, based on current weather [4]. Rating in medium and short OHLs is commonly determined by catenary sag [5], a limit given by a maximum temperature in the conductor. Hence, DLR is typically used for this kind of OHL.

Traditionally, line ratings are fixed according to extreme climate conditions that rarely occur. However, thanks to the development of information technologies, it is possible to compute online OHL's rating, via measurements of atmospheric conditions and current intensity. Two types of measurements for DLR have been defined, they are called direct and indirect [6]. The indirect method uses weather stations near to the OHLs whereas direct methods use sensors of mechanical tension, temperature, sag or measurements derived from these three variables. Devices used in direct methods are located directly in the OHL, making it difficult to put them into operation and requiring maintenance. Despite this, DLR exhibits low costs and it is fast to implement if compared with other methods used to increase OHL's ampacity [7]. Additionally, DLR is useful when it is necessary to increase the capacity between 10 and 30%, particularly for wind power integration [8], given the relationship between wind speed, power generation, and cooling. In brief, DLR increases the capacity of OHL most of the time, achieving asset optimisation.

The use of phasor measurement units (PMUs) allows the estimation of OHL's conductor thermal capacity in real time. This

method is considered as DLR technology, with the advantage that it uses an existing infrastructure capable of guaranteeing the functioning and reliability of the DLR system [9]. With PMU, conductor rating is estimated using impedance of OHL equivalent circuit [10, 11], because of impedance changes according to conductor temperature. This temperature impacts state estimation [12] and load flow [13], thereby affecting losses, bus voltages, protections schemes [14] and OHL ampacity, among others.

The use of PMU for DLR is based on the computing of OHL's average conductor temperature. However, conductor temperature varies along OHL, as a consequence of atmospheric variations in the different spans. Cecchi *et al.* [15] present a methodology for incorporating temperature variations along OHLs. This methodology consists of dividing the line into segments based on temperature gradients obtained from measurements along the conductor. In the same way, in [16] critical spans for monitoring OHLs are estimated by means of weather forecasting models, considering climate variations in time and space. However, there is no literature on the assessment of the error obtained by using resistance to compute OHL's conductor temperature.

This study proposes a methodology which consists in analysing, through simulations and analytically, the influence of measurement errors and atmospheric variations in time as well as space in the estimation of conductor temperature when PMUs are used. This methodology can be used to assess PMU for computing OHL's conductor temperature. This is in order to ensure that the estimated temperature error does not exceed acceptable margins. This paper is organised as follows: Section 2 discusses multiphysics behaviour of OHLs when changes in weather or load occur. In Section 3, the proposed expressions to compute error propagation are addressed when synchrophasors are used. Section 4 describes the OHL under study and the interpolation method used to compute atmospheric conditions along an OHL. In Section 5, the impact of weather over conductor temperature is computed in each ruling span and compared with the temperature calculated using PMU

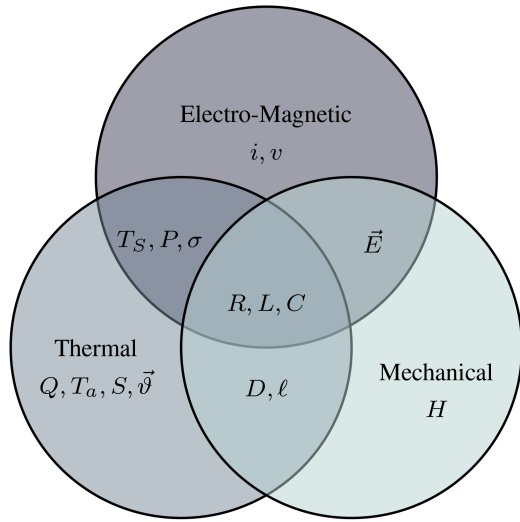


Fig. 1 Multiphysical phenomena in OHLs as a result of heat transfer

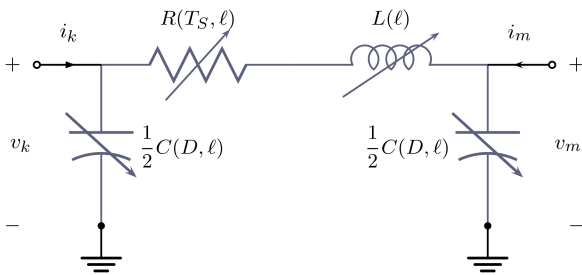


Fig. 2 Mechanical and thermal variables that influenced RLC parameters of an OHL modelled by π equivalent circuit

measurements. Finally, Section 6 analyses the error in estimation both OHL resistance and temperature when PMU measurements are used, taking into account measurement accuracy and load variations.

2 Multiphysics phenomena – background

During operation, OHLs are under influence of thermal, mechanical and electrical phenomena [17]. Fig. 1 shows the relationship between these physical phenomena. At first, a heat transfer (Q) is presented as a product of a heat gain (mainly by Joule effect (P) and solar radiation (S)) and a heat loss (radiation and convection). That heat transfer is determined by the current intensity (i_{kml}), conductor properties and atmospheric conditions (ambient temperature (T_a), solar radiation, and wind speed and direction (θ)). Heat transfer affects the conductor temperature (T_S), leading to a variation in the horizontal component of conductor mechanical tension (H), as a result of changes in conductor length (ℓ) and catenary sag (D). Additionally, changes in T_S , D , ℓ impact both electric field (\vec{E}) distribution and conductor electrical conductivity (σ). These variations reflect in the values of voltage (v) and current intensity (i) in OHL's. Finally, these three physical phenomena affect the OHL's RLC parameters, given that these parameters depend on line geometry and conductor properties.

2.1 Thermal phenomena

CIGRE [18] and IEEE [19] standards are commonly used for computing temperature in OHL conductors. These standards are based on the heat balance equation. For thermal steady state, (1) is used

$$Q_J + Q_S = Q_C + Q_R, \quad (1)$$

where Q_J is the heat gain from the Joule effect, Q_S is the gain from solar radiation, Q_C is the loss for convective cooling and Q_R is the loss for radiative cooling. The gain from magnetic heating and

corona heating, as well as the losses due to evaporative cooling, are commonly ignored.

From (1), the conductor temperature T_S and the maximum current intensity can be computed, provided that atmospheric conditions, current intensity and conductor properties (resistivity, the temperature coefficient of resistance, the solar absorptivity of the surface, the solar emissivity of the surface, diameter, among others) are known.

2.2 Mechanical phenomena

Temperature variations in conductors result in changes in their length and on forces that act on catenary. To model this behaviour, numerical or analytic formulations can use. Numerical methods such as finite elements are not commonly used for DLR, because they require specialised software and large computational resources when compared with analytical approximations. As an analytical method, the state change (2) approximates the mechanical tension in an OHL stringing section using the ruling span method [20, 21]

$$\frac{EA(r_s m_c g)^2}{24} = H^2 \left[H - H_{T_{ref}} + \frac{EA(r_s m_c g)^2}{24H_{T_{ref}}^2} + EA\epsilon_t(T_S - T_{ref}) \right]. \quad (2)$$

Equation (2) relates the tension H_S at a temperature T_S by means of a known $H_{T_{ref}}$ at a known temperature T_{ref} , where E is the modulus of elasticity of the conductor, A is the conductor cross section, g is the gravitational constant, m_c is the conductor mass per unit length, r_s is the equivalent ruling span length, and ϵ_t is the coefficient of thermal expansion. ϵ_t is a function of the stress and the elastic modulus. This dependence has a considerable influence at high temperatures [21]; however, in this research, it is assumed constant because the temperatures assumed in the simulations are below 25°C. Finally, as the values of $H_{T_{ref}}$ and ϵ_t vary over time, a continuous estimation of these values is necessary.

The conductor length per phase (ℓ) can be computed using OHL geometry and tension (H) by means of

$$\ell = \sqrt{h^2 + \left[\frac{2H}{m_c g} \sinh\left(\frac{m_c g s}{2H}\right) \right]^2}, \quad (3)$$

where h is the vertical distance between support elevation points (inclined spans) and s is the span length.

Finally, the OHL sag (D) is computed by

$$D = \frac{H}{m_c g} \left[\cosh\left(\frac{m_c g s}{2H}\right) - 1 \right]. \quad (4)$$

2.3 Electro-magnetic phenomena

The electrical parameters of the π equivalent circuit (Fig. 2) by which the electro-magnetic phenomena can describe are used for modelling OHLs with medium length. These parameters are influenced by variations both in load and weather as follows.

The equivalent conductor resistance (R) varies according to temperature (T_S) and conductor length (ℓ). These variations can be described by

$$R_{T_S} = R_{T_{ref}} (1 + \alpha(T_S - T_{ref})) \frac{\ell_{T_S}}{\ell_{T_{ref}}}, \quad (5)$$

where α is the resistance temperature coefficient. This equation is valid as long as the conductivity of the material is in the linear zone regarding temperature dependence, which occurs in the normal operation of OHLs.

The equivalent inductance (L) depends on conductor's arrangement, distances among them, and length of phase conductor. This parameter can be computed using

$$L = 2 \times 10^{-4} \ln \left(\frac{\text{GMD}}{\text{GMR}} \right) \ell, \quad (6)$$

where GMD is the geometric mean distance and GMR is the geometric mean radius.

The length of the phase conductor and the average distance (h_{avg}) between the conductor and ground influences the equivalent capacitance (C). To calculate C from geometry, (7) can use [5]

$$C = \frac{0.05556 \times 10^{-6}}{\ln(k_1(\text{GMD}/\text{GMR}_c))} \ell, \quad (7)$$

where k_1 depends on h_{avg} . Tleis [22] used (8) for computing h_{avg}

$$h_{\text{avg}} = \frac{\sqrt{(2h_M - D_{\text{avg}})D_{\text{avg}}}}{\log\left(\frac{h_M + \sqrt{(2h_M - D_{\text{avg}})D_{\text{avg}}}}{(h_M - D_{\text{avg}})}\right)}, \quad (8)$$

where D_{avg} is the average sag and h_M is the conductor height at the tower. This expression takes into account sag variation which is a function of temperature.

3 Error propagation

In this study, expressions to compute error propagation are proposed, provided that PMU measurements are used to estimate conductor temperature.

The sensibility on the computation of temperature using resistance is given by influence of the coefficient α as follows:

$$T_S = \frac{1}{\alpha} \left(\frac{R'_{T_S}}{R'_{T_{\text{ref}}}} - 1 \right) + T_{\text{ref}}. \quad (9)$$

Thus, the error propagates according to

$$\sigma_{T_S} = \frac{dT_S}{dR'_{T_S}} \sigma_R = \frac{1}{\alpha R'_{T_{\text{ref}}}} \sigma_R. \quad (10)$$

The value of σ_R depends on the devices accuracy as well as load and impedance of OHL. The impact of the load in the estimation of temperature is explained by means of error propagation on the measurements. To carry out this analysis, it is assumed that the influence of the OHL capacitance is negligible, obtaining

$$R \simeq \text{Re} \left(\frac{v_k - v_m}{i_{km}} \right). \quad (11)$$

Thus, the uncertainty is propagated according to

$$\begin{aligned} \sigma_R &= \sqrt{\left(\frac{\partial R}{\partial v_k} \sigma_v \right)^2 + \left(\frac{\partial R}{\partial v_m} \sigma_v \right)^2 + \left(\frac{\partial R}{\partial i_{km}} \sigma_{i_{km}} \right)^2}, \\ \frac{\partial R}{\partial v_k} &= \frac{\cos(\angle v_k - \angle i_{km})}{|i_{km}|}, \\ \frac{\partial R}{\partial v_m} &= -\frac{\cos(\angle v_m - \angle i_{km})}{|i_{km}|}, \\ \frac{\partial R}{\partial i_{km}} &= \frac{|v_k| \cos(\angle v_k - \angle i_{km}) - |v_m| \cos(\angle v_m - \angle i_{km})}{|i_{km}|^2}. \end{aligned} \quad (12)$$

4 Case study

To analyse the impact of both weather and PMU measurement errors in the estimation of OHL's RLC parameters and conductor temperature, this work studies the OHL identified as BR1 that belongs to the Icelandic transmission system operated by Landsnet. This OHL connects geothermal plants and the substation Brennimerur, and it is considered as the most critical connection in the country [23]. As shown in Fig. 3, BR1 connection crosses mountains, valleys and the sea, and it was built with three different types of conductors; therefore, temperature variations along the

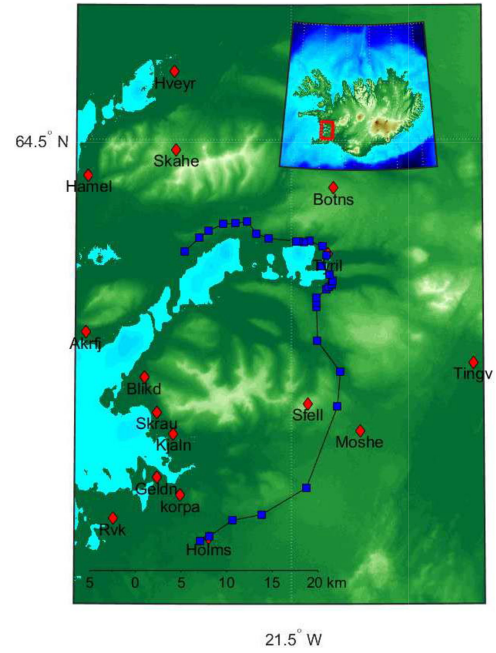


Fig. 3 Geographic location of BR1-OHL ruling spans (blue squares) and nearby weather stations (red diamonds)

conductor occur. Given these characteristics, DLR is an option to increase the reliability and capacity of BR1-OHL.

4.1 Test line

BR1 has a rate voltage of 220 kV, a length of 59.4 km and it is suspended at 172 towers divided into 30 tension sections shown in Table 1. In this work, each stringing section is approached through a ruling span [21]. Different types of conductors are used on the OHL; their properties are shown in Table 2. Weather conditions for static rating are: ambient temperature $T_a = 10^\circ\text{C}$, wind speed and attack angle $\theta_a = 0.6 \angle 90^\circ$ m/s and solar radiation $S = 0 \text{ W/m}^2$ for an allowable conductor temperature $T_s = 40^\circ\text{C}$.

4.2 Weather nowcasting

To compute conductor temperature in each ruling span, this work assumes that atmospheric conditions do not change along each ruling span. Thus, atmospheric conditions were interpolated through biharmonic splines, evaluating the points located in the middle of each ruling span using records and location of weather station and the function *griddata* of Matlab[®]. An accurate model of weather nowcasting is beyond the scope of this study, because this work only seeks to analyse the influence of weather variations as well as PMU measurement errors on the estimation of conductor capacity. There are 16 weather stations close to BR1-OHL; their names and locations are shown in Table 3. The measurement records from these stations are available online at the Icelandic Met Office webpage. For DLR, it is recommended to take 10 or 15 average and standard deviation of samples [24]. However, as the aim of this study is to evaluate the performance to use PMU for DLR, the atmospheric conditions between 2016-04-18 00:00 and 2016-04-18 21:00, with samples taken every three hours, were considered. As example, temperature and wind interpolations for the date 2016-04-18 21:00 are shown in Fig. 4. Given the climate characteristics of Iceland, solar radiation is neglected [23] and normally the Icelandic Met Office does not report this parameter.

5 Impact of atmospheric variations

To analyse the impact of atmospheric variations on the BR1-OHL capacity, thermal, mechanical and electrical variables were calculated for each ruling span using weather interpolation and OHL geometry. Fig. 5 shows the flowchart for computing the values of these variables (T_s, ℓ, S, H, R, L, C). Afterwards, in order

Table 1 BR1 OHL – stringing section characteristics

Ruling span	Conductor type	Capacity, MVA	Spans length, m
1	470-AL3	304	289, 387, 440
2	470-AL3	304	230, 395, 302, 308, 392, 410, 337, 336, 359
3	470-AL3	304	436, 398, 457, 340, 277, 188, 432, 268, 187, 331
4	470-AL3	304	421, 343, 394, 408, 308, 397, 414, 313, 376, 435, 435, 436, 405, 208, 394
5	470-AL3	304	318, 449, 386, 414, 386, 441, 413, 402, 441, 410, 416, 433, 405, 431, 395, 444, 408, 428, 391, 367, 353, 342, 349, 375
6	470-AL3	304	379, 453, 317, 299, 411, 328, 450, 418, 416, 308
7	470-AL3	304	388, 389, 446, 429, 433, 293, 377, 446, 372, 446, 225
8	470-AL3	304	387, 389, 294, 224, 241, 455, 272, 398, 414, 366, 398, 354, 252
9	470-AL3	304	426
10	470-AL3	304	197, 213, 194
11	470-AL3	304	208, 140, 136, 183, 162, 136, 142, 146, 133
12	470-AL3	304	400
13	470-AL3	304	392
14	470-AL3	304	480
15	470-AL3	304	272, 295, 192
16	6469-AL3134ST4A	304	202, 909, 159
17	470-AL3	304	318, 278, 371, 329
18	470-AL3	352	316, 316, 233, 217
19	470-AL3	304	258, 383, 327, 374, 255
20	470-AL3	304	377, 182
21	470-AL3	304	270, 284
22	470-AL3	304	312
23	470-AL3	304	380, 290, 362, 378, 388, 349, 303, 280, 341
24	470-AL3	304	373, 329, 365, 347
25	774-AL3	304	468, 329, 289, 580
26	2X774-AL3	415	222, 349, 337, 387
27	2X774-AL3	830	441, 249, 288, 349
28	2X774-AL3	830	193, 398, 307, 238, 351, 316
29	2X774-AL3	830	173, 260, 276, 213, 297
30	2X774-AL3	830	368, 384, 398, 385, 337, 340

to evaluate PMU performance, these results are compared with the values computed using synchrophasors' simulations. These simulations are assumed at the ends of the OHL. Thus, with the phasor simulations of v_k, i_k, v_m, i_m and with (13) and (14), the average temperature T_S is computed through the estimation of circuit parameters of Fig. 2

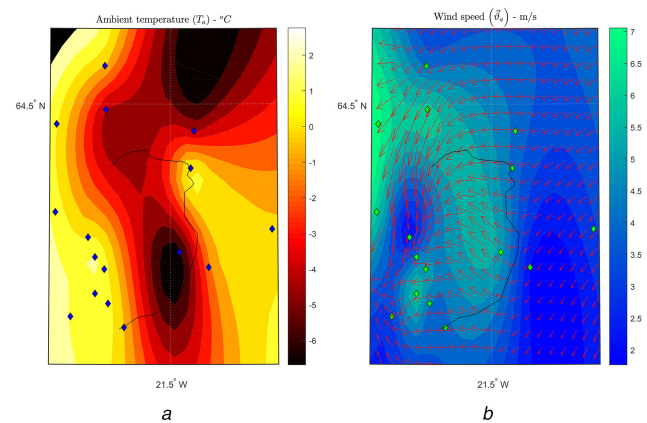
$$Z = \frac{v_k^2 - v_m^2}{v_m i_k - v_k i_m}, \quad (13)$$

Table 2 BR1 OHL conductors

	470-AL3	6469-AL3/134ST4A	774-AL3	Unit
type	aluminium conductor alloy reinforced (ACAR)	aluminium conductor steel-reinforced (ACSR)	ACAR	—
A	469.6×10^{-6}	469×10^{-6}	774.2×10^{-6}	m ²
m_c	1.294	2.4217	2.140	kg/m
E	$57,000 \times 10^6$	$67,100 \times 10^6$	$55,000 \times 10^6$	N/m ²
ϵ_t	23×10^{-6}	19.3×10^{-6}	23×10^{-6}	1/K
$R'_{T_{ref}}$	0.07415×10^{-3}	0.0768×10^{-3}	0.0389×10^{-3}	Ω/m
α	0.0036	0.0038	0.0036	1/K
T_{ref}	25	20	20	°C
α_s	0.5	0.5	0.5	1
ϵ	0.5	0.5	0.5	1
D	28.14×10^{-3}	32.28×10^{-3}	36.18×10^{-3}	m

Table 3 Weather station close to the BR1 influence area

Weather station	WMO number	Latitude, °	Longitude, °
Rvk	04030	64.1275	-21.9028
Holms	04920	64.1085	-21.6864
Korpa	04132	64.15049	-21.75109
Geldn	04880	64.1678	-21.8038
Kjaln	04848	64.2106	-21.7667
Skrau	04818	64.2318	-21.8046
Blikd	04912	64.2664	-21.8329
Sfell	04136	64.2405	-21.4633
Moshe	04918	64.214	-21.3448
Tingv	04142	64.2807	-21.0875
Akrfj	04926	64.3105	-21.966
Tyrl	04806	64.3877	-21.4169
Botns	04814	64.4529	-21.4034
Skahe	04904	64.4902	-21.7621
Hamel	04128	64.4647	-21.9628
Hveyr	04134	64.567	-21.767

**Fig. 4** Weather nowcasting for the area of influence of BR1 OHL, at 2016-04-18 21:00

(a) Temperature,
(b) Wind speed

$$Y = \text{Im} \left(2 \cdot \frac{i_k + i_m}{v_k + v_m} \right). \quad (14)$$

The current intensity i_{km} used to compute the OHL parameters is given by

$$i_{km} = i_k - \frac{v_k Y}{2}. \quad (15)$$

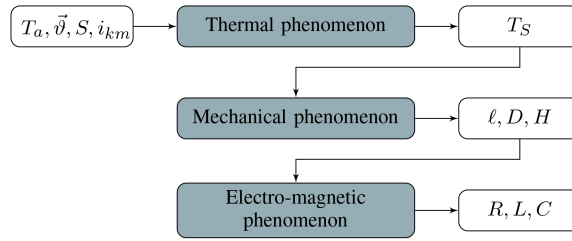


Fig. 5 Flowchart to compute each OHL parameter which varies with the weather and current intensity

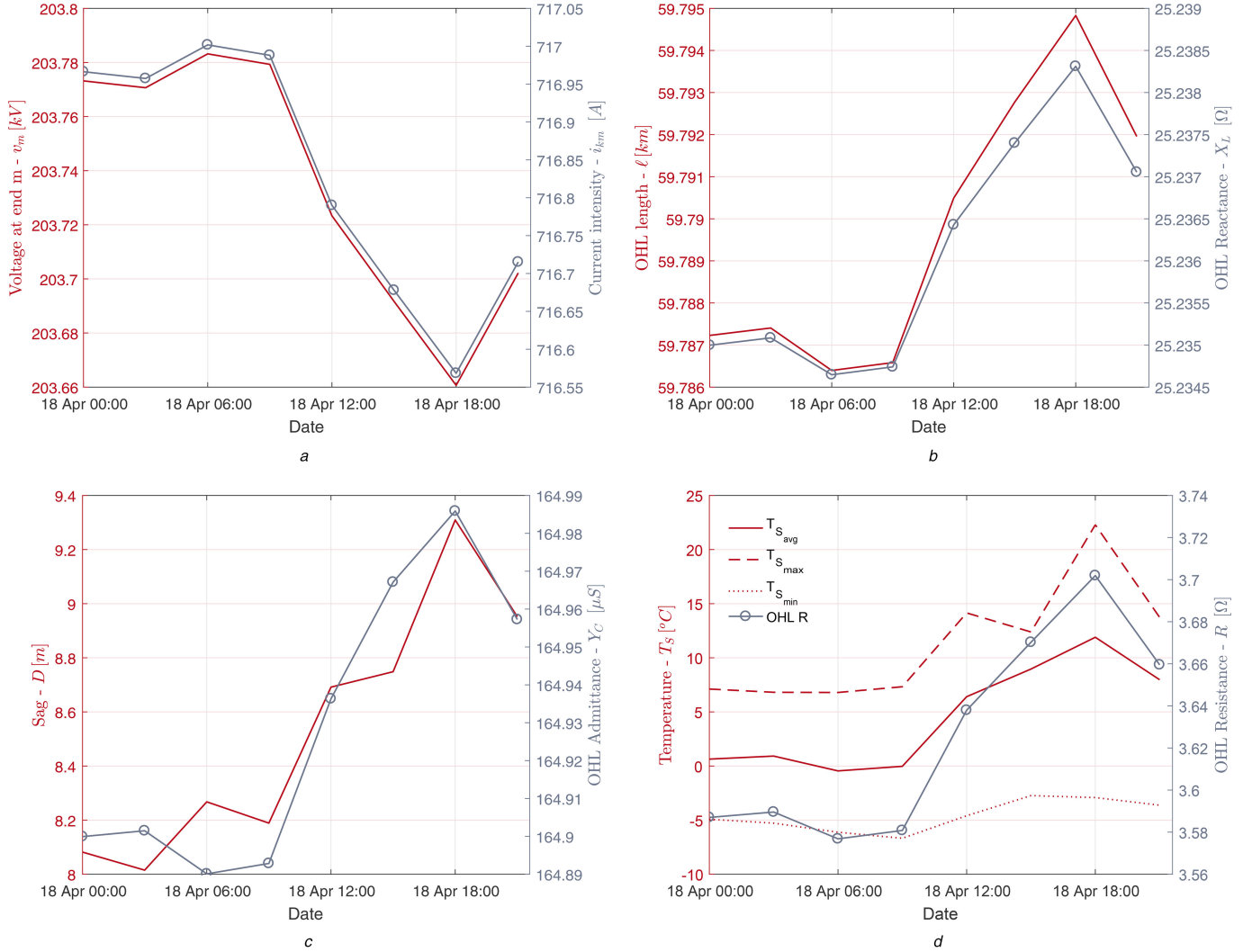


Fig. 6 Variation of the parameters of the BRI-OHL for each weather sample

- (a) Current intensity (i_{km}) flowing through the OHL and voltage at end m (v_m),
 (b) Inductance (reactance) and phase conductor length,
 (c) Capacitance (admittance) and sag of ruling span number 8,
 (d) Resistance, average temperature and, maximum and minimum temperature along the OHL

PMU values were simulated with SIMULINK[®] as follows: a power flow for the circuit of Fig. 2 is run initially assuming design values of resistance, inductance and capacitance under rate conditions, $v_k = 220$ kV, $S = 304$ MVA and PF = 0.9. Afterwards, an iterative script was implemented changing the RLC values of the π model according to (5)–(7), with the aim of updating the electrical parameters considering the changes in conductor temperature. This script runs until the current intensity computed through the load flow is equal to the current i_{km} used for calculating the resistance from (5). As simulations results, Fig. 6 shows variations of the ℓ , X_L , Y_C , R , D and T_s parameters for each weather sample. These values are of the entire OHL except D which is the sag of the ruling span number 8. This span was chosen because it has the highest variation within samples, ~ 1.3 m. Thus, weather influence over the sag can be determined.

In Fig. 6a are shown the values both of current intensity i_{km} and of voltage v_m obtained for each sample. The maximum variation of the entire phase conductor length is $<0.02\%$, which corresponds to 9 m. This means that the OHL inductance is not affected as a consequence of typical atmospheric variations. Therefore, the phase conductor length can be assumed constant, as shown in Fig. 6b. In the same way, the variation between the maximum and minimum value of the equivalent capacitance is $<0.2\%$, exhibiting negligible influence of the sag (D), as shown in Fig. 6c. On the other hand, the resistance changes up to 3.5%, as shown in Fig. 6d. In Fig. 6d, the average conductor temperature ($T_{s,avg}$) is computed using the resistance, obtaining a maximum and minimum of 6.7 and 2.6 $^{\circ}C$, respectively. In all samples, the differences between $T_{s,avg}$ and $T_{s,max}$ exceeded the acceptable error margin for critical spans of 4 K (10% of 40 $^{\circ}C$) proposed in [6]. The maximum temperature

($T_{S_{\max}}$) and minimum temperature ($T_{S_{\min}}$) were obtained by computing the temperature from the weather in all ruling spans and taking the highest and lowest of these values.

As a consequence of using different conductors in BR1-OHL, the value of T_S in each ruling span varies, even if the weather does not change along with it. In this work, this is considered by using the following procedure: an equivalent temperature ($T_{S_{\text{avg}}}$) is computed with (16) using the resistance (R_{equiv}) calculated with (5).

$$T_{S_{\text{avg}}} = \frac{R_{\text{equiv}} - \sum_{i=1}^N R_i(T_{\text{ref}}) + \sum_{i=1}^N R_i(T_{\text{ref}}) \cdot \alpha_i \cdot T_{\text{ref}}}{\sum_{i=1}^N R_i(T_{\text{ref}}) \cdot \alpha_i}. \quad (16)$$

With this equivalent temperature and supposing initial values of average ambient temperature ($T_{a_{k=0}}$) and solar radiation, an equivalent cooling heat is computed. With this parameter, an equivalent wind speed ($\vec{\vartheta}_{\text{equiv}}$) is calculated [25] along the entire OHL. With these new atmospheric conditions, the temperature in each ruling span (T_{S_i}) is calculated, thus the resistivity of each conductor is considered. However, as T_a is originally guessed, it is necessary to adjust this value via iterations until the difference between the weighted average of (T_{S_i}) and ($T_{S_{\text{avg}}}$) is less than an error (ϵ). This procedure is shown in Fig. 7.

Fig. 8 shows both the temperature and error were calculated under atmospheric conditions in each ruling span and the temperature computed using simulations of PMU measurements. Fig. 8a shows a dynamic behaviour in time and space (along the OHL) of the conductor temperature. Moreover, the critical ruling span changes for each weather sample, and the acceptable error margin of (4 K) is exceeded between the different critical spans, as shown in Fig. 8b. The critical span was assumed as the span with the highest temperature.

6 PMU measurement error impact

6.1 Impact on the accuracy

In this section, conductor's temperature is estimated considering errors in PMU measurements. Measurement errors were simulated assuming a random normal distribution of error with mean zero and standard deviation approximated to 1/3 of meter accuracy. A typical accuracy of 0.3% was assumed for measurement simulations for both current and voltage [26]. The angle between phasors was taken without error; this is analysed in [27]. Additionally, the estimation algorithm proposed in [10] was implemented in order to reduce the error in the computing of OHL resistance and average conductor temperature.

For each weather sample, 1000 simulations were run by adding normal random errors to PMU measurements of v_k, i_k, v_m, i_m . Random errors were simulated with Matlab®. Fig. 9a shows the measurement error impact on the resistance estimation, obtaining an uncertainty of ~16%. The uncertainty in this work is assumed as three times the standard deviation (σ). This uncertainty is equivalent to an error within $\pm 0.6 \Omega$, considering a normal distribution with a mean between 3.6 Ω and 3.7 Ω . Thus, the error in the estimation of the equivalent resistance per unit length (R'_{eqv}) is within $\pm 10 \times 10^{-3} \Omega/\text{km}$. This error propagates to the computing of temperature, reaching errors within $\pm 38 \text{ K}$, as shown in Fig. 9b.

In the case studies, the 470-AL3, 6469-AL3 /134ST4A and 774-AL3 conductors, which are used in BR1-OHL, the errors calculated by (10) are within $\pm 37, \pm 34$ and $\pm 36 \text{ K}$, respectively. These values are close to the values shown in Fig. 9b. The differences are due to the use of R'_{equiv} for computing the standard deviation σ_r .

7 Impact of load on the estimation of conductor temperature

As voltage and current magnitudes depend on load and OHL impedance, the latter influences the resistance estimation, and therefore, the computing of conductor temperature. A simulation

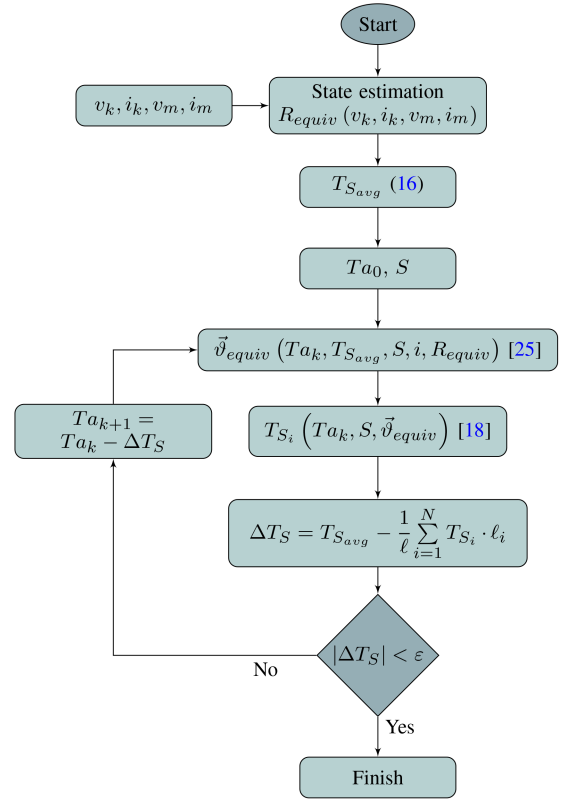


Fig. 7 Flow chart for computing T_S in each ruling span using PMU measurements

like the one of the previous section is carried out for the weather sample 2016-04-18 21:00, changing the load between 0.1 and 1 pu and the power factor (PF) between 0.1 and 0.95. The simulation results are shown in Fig. 10. The standard deviation σ was calculated with the 500 runs for each set of loads and PFs. In the estimation of the equivalent resistance (R_{equiv}) and the computing of conductor temperature T_S , the minimum standard deviation was 0.027 Ω and 1.9 K, respectively, for a PF of 0.1 and a load of 1 pu. The maximum standard deviation was 2.41 Ω and 172 K for a PF of 0.95 and a load of 0.1 pu.

Given that $\sigma_R \propto 1/i_{km}$ in (10), the uncertainty in the computing of temperature is increased at low power flows. Additionally, if the PF is approximated to $\cos \angle i_{km}$ (using $\angle v_k = 0$ as reference, $\angle v_m$ close to $\angle v_k$ and $\angle i_{km}$ measured with respect to $\angle v_k$) the uncertainty increases as PF is close to 1. On the other hand, a typical ratio between magnitudes of voltage (kV) and current (A) in power transmission systems impacts the measurement error in resistance computing.

The simulation results of this study were not contrasted with real PMU's measurements at the same time. However, Sun *et al.* [2] report results about the use of PMU measurements in the studied BR1-OHL. The temperature obtained was outside the acceptable error margins. Additionally, Carlini *et al.* [28] report high variation including negative values in the computation of the resistance in a real OHL when PMU measurements are used. Both results are consistent with those obtained in this study. Therefore, using the proposed methodology, the PMU performance could be predicted.

8 Discussion

Based on both the weather variations along OHLs and error in PMU measurements, a methodology to assess the use of synchrophasors as the DLR method was introduced. Its main advantage is to use simulations and expressions to evaluate the performance of PMU for DLR during the planning stage. For instance, as a result of using this methodology in the case study in this work, the BR1-OHL capacity cannot be estimated using PMU. Thus, applying this methodology would reduce costs by avoiding future fail implementations. However, provided that a successful

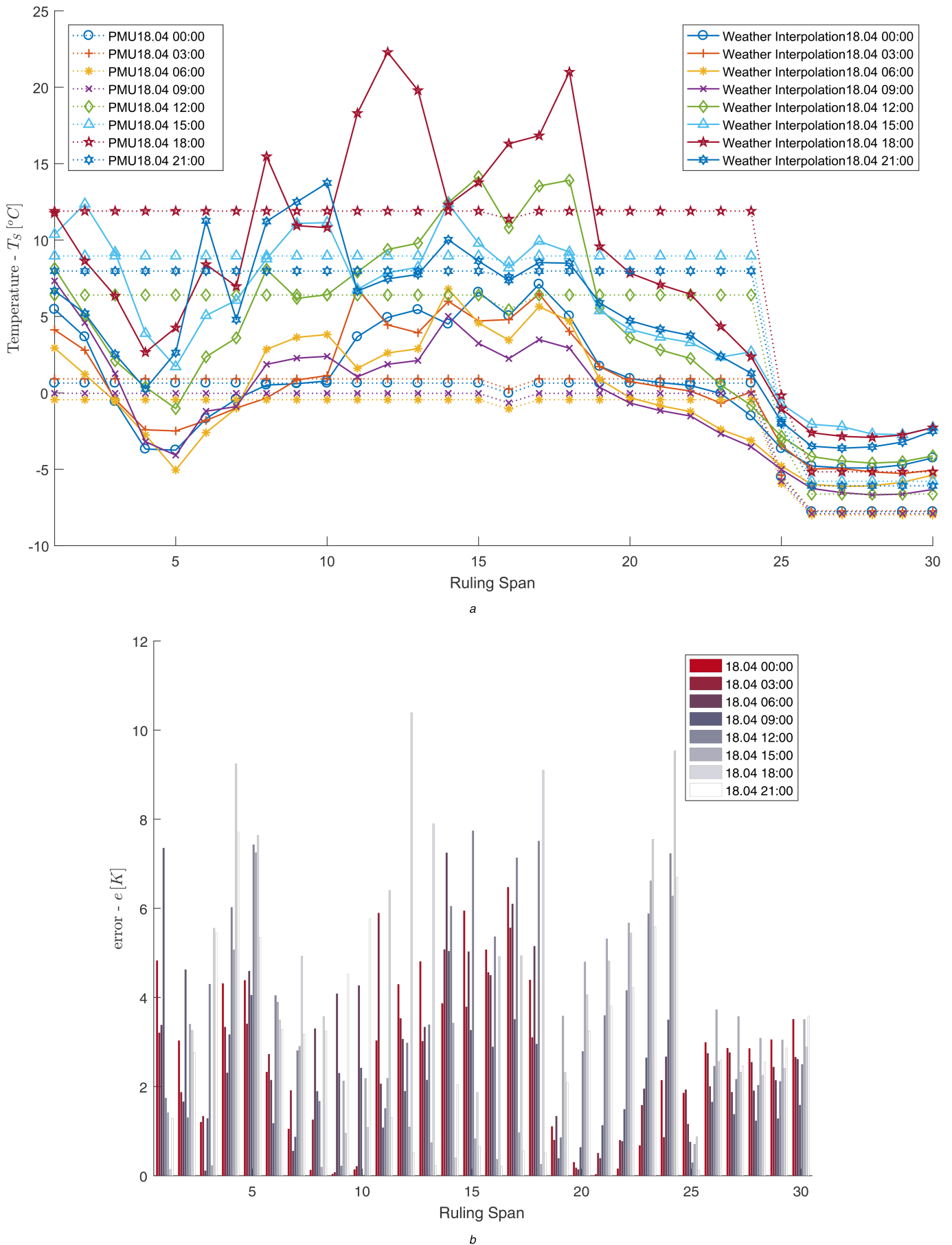


Fig. 8 Comparison between temperatures computed using weather interpolation and using PMU estimation in each ruling span for different times
 (a) Temperature of the conductor $-T_s$,
 (b) Error between T_s computed using weather interpolation and PMU estimation

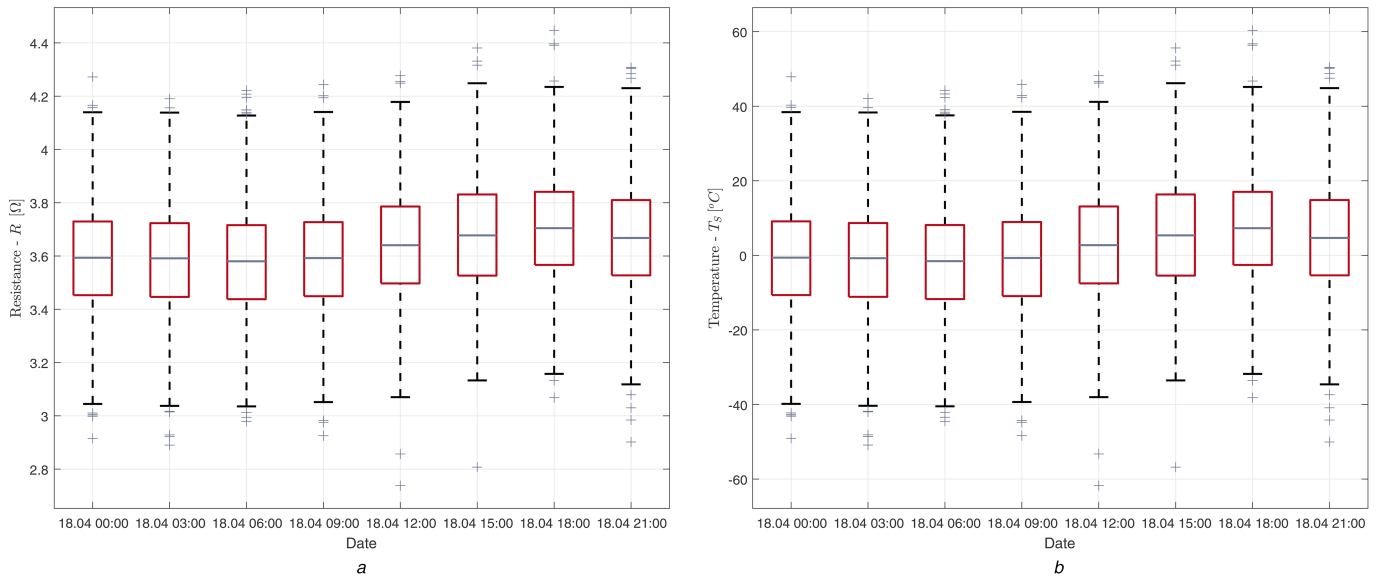


Fig. 9 Box plots with the value of both OHL resistance and $T_{s_{avg}}$ estimated using PMU for each sample, assuming an accuracy of 0.3% in simulations of voltage and current measurements

(a) OHL resistance,

(b) Average temperature of the conductor - $T_{s_{avg}}$

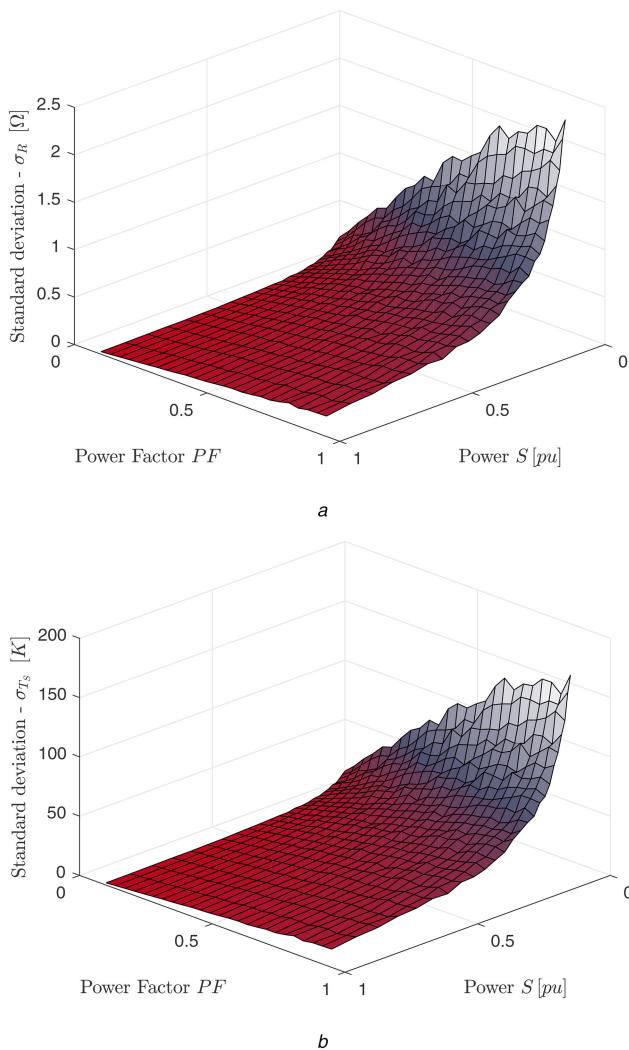


Fig. 10 Influence of load on the estimation of both conductor's resistance and temperature using PMU measurements

(a) OHL's resistance,

(b) Average conductor temperature - $T_{s_{avg}}$

result of applying the proposed methodology is achieved, further analysis and validation must be carried out before implementing PMU as the DLR method. This analysis should include the presence of uncorrelated data as well as bad data and a more accurate model to describe stringing sections given the limitation of ruling span approximation, mainly at high operating temperatures.

9 Conclusions

The changes in the load and atmospheric conditions along an OHL result in alteration of thermal and mechanical variables, which affect the electrical RLC parameters. This influence is negligible for inductance and capacitance under typical atmospheric and load conditions, as a consequence of the small variation of the line length and low impact of the sag on the capacitance. On the contrary, the value of the resistance changes in a non-neglected way.

The use of PMU's measurements for DLR faces challenges when atmospheric conditions and conductor properties change along OHLs, together with inaccuracy, due to the error propagation in the computation of resistance. Thus, the average value of temperature computed from PMU measurements could not depict the real conductor capacity and jeopardises OHL, as shown in this study. This has a consequence of exceeding accepted security margins in critical spans if the temperature computed with synchrophasors is used. Additionally, the estimated conductor's temperature error can be outside acceptable margins, as a result of the sensibility of temperature with resistance, even if state estimation algorithms are used. For these reasons, a methodology to assess the use of PMU for DLR is proposed. As future research, error minimisation techniques that account weather models, PMU and the monitoring of critical spans could potentially improve the estimation of conductor rating.

10 Acknowledgments

Authors thank LANDSNET-Iceland, for providing the test cases in section 4. This research was supported by the Colombian Department of Science, Technology and Innovation (Colciencias) under the project 617 – National Doctorates.

11 References

- [1] Winter, W., Elkington, K., Bareux, G., *et al.*: 'Pushing the limits: Europe's new grid: innovative tools to combat transmission bottlenecks and reduced

- inertia', *IEEE Power Energy Mag.*, 2015, **13**, (1), pp. 60–74. Available at <http://ieeexplore.ieee.org/document/6998972/>
- [2] Sun, W.Q., Zhang, Y., Wang, C.M., *et al.*: 'Flexible load shedding strategy considering real-time dynamic thermal line rating', *IET Gener. Transm. Distrib.*, 2013, **7**, (2), pp. 130–137. Available at <http://ieeexplore.ieee.org/document/6519364/>
 - [3] CIGRE WG B2.13: 'Guidelines for increased utilization of existing overhead transmission lines'. Technical Brochure 353 (CIGRE, Paris, France, 2008)
 - [4] Douglass, D., Chisholm, W., Davidson, G., *et al.*: 'Real-Time overhead transmission-line monitoring for dynamic rating', *IEEE Trans. Power Deliv.*, 2016, **31**, (3), pp. 921–927. Available at <http://ieeexplore.ieee.org/document/6991585/>
 - [5] Papailiou, K.O.: 'Overhead lines: a Cigre green book' (Cigre, Paris, France, 2014)
 - [6] CIGRE WG B2.36: 'Guide for application of direct real-time monitoring systems'. Technical Brochure 498 (CIGRE, Paris, France, 2012)
 - [7] International des grands réseaux électriques. Joint working group B2-C1 (19), C.: 'Increasing capacity of overhead transmission lines: needs and Solutions' (CIGRE, Paris, France, 2010). Available at <http://www.e-cigre.org/>
 - [8] Fernandez, E., Albizu, I., Bedialauneta, M.T., *et al.*: 'Review of dynamic line rating systems for wind power integration', *Renew. Sustain. Energy Rev.*, 2016, **53**, pp. 80–92
 - [9] Alvarez, D.L., Rosero, J.A., Faria da Silva, F., *et al.*: 'Dynamic line rating – technologies and challenges of PMU on overhead lines: A survey'. 2016 51st Int. Universities Power Engineering Conf. (UPEC), Coimbra, Portugal, September 2016, pp. 1–6. Available at <http://ieeexplore.ieee.org/document/8114069/>
 - [10] Du, Y., Liao, Y.: 'On-line estimation of transmission line parameters, temperature and sag using PMU measurements', *Electr. Power Syst. Res.*, 2012, **93**, pp. 39–45
 - [11] Rehtanz, C.: 'Synchrophasor based thermal overhead line monitoring considering line spans and thermal transients', *IET Gener. Transm. Distrib.*, 2016, **10**, (5), pp. 1232–1239
 - [12] Bockarjova, M., Andersson, G.: 'Transmission line conductor temperature impact on state estimation accuracy'. 2007 IEEE Lausanne Power Tech, Lausanne, Switzerland, July 2007, pp. 701–706. Available at <http://ieeexplore.ieee.org/lpdocs/epic03/wrapper.htm?arnumber=4538401>
 - [13] Frank, S., Sexauer, J., Mohagheghi, S.: 'Temperature-dependent power flow', *IEEE Trans. Power Syst.*, 2013, **28**, (4), pp. 4007–4018
 - [14] Sivanagaraju, G., Chakrabarti, S., Srivastava, S.C.: 'Uncertainty in transmission line parameters: estimation and impact on line current differential protection', *IEEE Trans. Instrum. Meas.*, 2013, **PP**, (99), p. 1
 - [15] Cecchi, V., Leger, A. S., Miu, K., *et al.*: 'Incorporating temperature variations into transmission-line models', *IEEE Trans. Power Deliv.*, 2011, **26**, (4), pp. 2189–2196
 - [16] Matus, M., Saez, D., Favley, M., *et al.*: 'Identification of critical spans for monitoring systems in dynamic thermal rating', *IEEE Trans. Power Deliv.*, 2012, **27**, (2), pp. 1002–1009. Available at <http://ieeexplore.ieee.org/document/6163401/>
 - [17] Mai, R., Fu, L., HaiBo, X.: 'Dynamic line rating estimator with synchronized phasor measurement'. 2011 Int. Conf. Advanced Power System Automation and Protection, vol. 2, Beijing, China, October 2011, pp. 940–945. Available at <http://ieeexplore.ieee.org/document/6180545/>
 - [18] Stephen, R., Douglas, D., Mirosevic, G., *et al.*: 'Thermal behaviour of overhead conductors' (CIGRE, Paris, France, 2002). Available at <http://www.e-cigre.org/>
 - [19] IEEE Std 738-2006: 'IEEE standard for calculating the current-temperature of bare overhead conductors'. 2007
 - [20] Motlis, Y., Barrett, J.S., Davidson, G.A., *et al.*: 'Limitations of the ruling span method for overhead line conductors at high operating temperatures', *IEEE Trans. Power Deliv.*, 1999, **14**, (2), pp. 549–560. Available at: <http://ieeexplore.ieee.org/document/754102/>
 - [21] CIGRE TF B2.12.3: 'Sag-tension calculation methods for overhead lines'. Technical Brochure 324 (CIGRE, Paris, France, 2007), p. 91
 - [22] Tleis, N.: 'Power systems modelling and fault analysis: theory and practice'. Newnes Power Engineering Series (Elsevier Science, Oxford, UK, 2007)
 - [23] Jiliusson, S.R.: 'Using PMU measurements to assess dynamic line rating of transmission lines'. M.Sc. Thesis in Electrical Power Systems and High Voltage Engineering, Aalborg University, 2013. Available at http://projekter.aau.dk/projekter/files/77194901/Dynamic_Line_Rating.pdf
 - [24] CIGRE WG B2.12: 'Guide for selection of weather parameters for bare overhead conductor ratings'. Technical Brochure 299 (CIGRE, Paris, France, 2006)
 - [25] Albizu, I., Fernandez, E., Eguia, P., *et al.*: 'Tension and ampacity monitoring system for overhead lines', *IEEE Trans. Power Deliv.*, 2013, **28**, (1), pp. 3–10. Available at <http://ieeexplore.ieee.org/document/6313952/>
 - [26] IEEE Std C57.13-2016: 'IEEE standard requirements for instrument transformers', *IEEE Std C57.13-2016 (Revision of IEEE Std C57.13-2008)*, 2016, pp. 1–96
 - [27] Zhao, J., Tan, J., Wu, L., *et al.*: 'Impact of measurement error on synchrophasor applications'. 2015. Available at <https://certs.lbl.gov/publications/impact-measurement-error>
 - [28] Carlini, E.M., Pisani, C., Vaccaro, A., *et al.*: 'Dynamic line rating monitoring in WAMS: challenges and practical solutions'. 2015 IEEE 1st Int. Forum on Research and Technologies for Society and Industry, RTSI 2015 – Proc., Turin, Italy, September 2015, pp. 359–364